Functional Quantum Nodes for Entanglement Distribution over Scalable Quantum Networks

Chin-Wen Chou, *et al.*

Science **316**, 1316 (2007);
DOI: 10.1126/science.1140300

Science (print ISSN 0036-8075; online ISSN 1095-9203) is published weekly, except the last week in December, by the American Association for the Advancement of Science, 1200 New York Avenue NW, Washington, DC 20005.

able degree of control over individual nuclear spins.

References and Notes

1. J. I. Cirac, P. Zoller, H. Mabuchi, H. J. Kimble, *Phys. Rev. Lett.* **78**, 3221 (1997).
2. A. Steane, D. Lucas, *Fortschr. Phys.* **48**, 839 (2000).
3. H. J. Briegel, W. Dür, J. I. Cirac, P. Zoller, *Phys. Rev. Lett.* **81**, 5932 (1998).
4. D. Gottesman, I. Chuang, *Nature* **402**, 390 (1999).
5. L. Duan, B. Blinov, D. Moehring, C. Monroe, *Quant. Inf. Comp.* **4**, 165 (2004).
6. S. C. Benjamin, D. E. Browne, J. Fitzsimons, J. J. L. Morton, *N. J. Phys.* **8**, 141 (2006).
7. L. Childress, J. M. Taylor, A. Sørensen, M. D. Lukin, *Phys. Rev. Lett.* **96**, 070504 (2006).
8. P. van Loock *et al.*, *Phys. Rev. Lett.* **96**, 240501 (2006).
9. L. Jiang, J. M. Taylor, A. S. Sorensen, M. D. Lukin, http://arxiv.org/abs/quant-ph/0703029 (2007).
10. D. Leibfried *et al.*, *Nature* **438**, 639 (2005).
11. H. Häffner *et al.*, *Nature* **438**, 643 (2005).
12. B. Blinov, D. L. Moehring, L. M. Duan, C. Monroe, *Nature* **428**, 153 (2004).
13. P. Maunz *et al.*, http://arxiv.org/abs/quant-ph/0608047 (2006).
14. J. Wrachtrup, S. Y. Kilin, A. P. Nizovtsev, *Opt. Spectrosc.* **91**, 429 (2001).
15. F. Jelezko, T. Gaebel, I. Popa, A. Gruber, J. Wrachtrup, *Phys. Rev. Lett.* **92**, 076401 (2004).
16. T. Gaebel *et al.*, *Nature Phys.* **2**, 408 (2006).
17. R. Hanson, F. Mendoza, R. J. Epstein, D. D. Awschalom, *Phys. Rev. Lett.* **97**, 087601 (2006).
18. R. J. Epstein, F. M. Mendoza, Y. K. Kato, D. D. Awschalom, *Nat. Phys.* **1**, 94 (2005).
19. J. R. Petta *et al.*, *Science* **309**, 2180 (2005); published online 1 September 2005 (10.1126/science.1116955).
20. F. H. L. Koppens *et al.*, *Nature* **442**, 766 (2006).
21. L. Childress *et al.*, *Science* **314**, 281 (2006); published online 13 September 2006 (10.1126/science.1131871).
22. B. Kane, *Nature* **393**, 133 (1998).
23. L. M. K. Vandersypen, I. L. Chuang, *Rev. Mod. Phys.* **76**, 1037 (2004).
24. C. Negrevergne *et al.*, *Phys. Rev. Lett.* **96**, 170501 (2006).
25. F. Jelezko *et al.*, *Phys. Rev. Lett.* **93**, 130501 (2004).
26. See supporting material on *Science* Online.
27. S. Massar, S. Popescu, *Phys. Rev. Lett.* **74**, 1259 (1995).
28. J. Rabeau *et al.*, *Appl. Phys. Lett.* **88**, 023113 (2006).
29. M. D. Lukin, P. R. Hemmer, *Phys. Rev. Lett.* **84**, 2818 (2000).
30. P. Tamarat *et al.*, *Phys. Rev. Lett.* **97**, 083002 (2006).
31. C. Santori *et al.*, *Phys. Rev. Lett.* **97**, 247401 (2006).

32. We thank P. Cappellaro, J. Doyle, N. Khaneja, C. Marcus, A. Mukherjee, J. Taylor, and J. Wrachtrup for many stimulating discussions and experimental help, and S. Prawer for providing high-purity diamond samples. Supported by NSF (CAREER and Physics at the Information Frontier), the Army Research Office, the Packard and Hertz Foundations, Deutsche Forschungsgemeinschaft grant SFB/TR21, and the European Commission (F.J.).

Supporting Online Material

www.sciencemag.org/cgi/content/full/316/5829/1312/DC1
Materials and Methods
SOM Text
Figs. S1 and S2
References

11 January 2007; accepted 11 April 2007
10.1126/science.1139831

Functional Quantum Nodes for Entanglement Distribution over Scalable Quantum Networks

Chin-Wen Chou, Julien Laurat, Hui Deng, Kyung Soo Choi, Hugues de Riedmatten,* Daniel Felinto,† H. Jeff Kimble‡

We demonstrated entanglement distribution between two remote quantum nodes located 3 meters apart. This distribution involves the asynchronous preparation of two pairs of atomic memories and the coherent mapping of stored atomic states into light fields in an effective state of near-maximum polarization entanglement. Entanglement is verified by way of the measured violation of a Bell inequality, and it can be used for communication protocols such as quantum cryptography. The demonstrated quantum nodes and channels can be used as segments of a quantum repeater, providing an essential tool for robust long-distance quantum communication.

In quantum information science (*1*), distribution of entanglement over quantum networks is a critical requirement for metrology (*2*), quantum computation (*3*, *4*), and communication (*3*, *5*). Quantum networks are composed of quantum nodes for processing and storing quantum states, and quantum channels that link the nodes. Substantial advances have been made with diverse systems toward the realization of such networks, including ions (*6*), single trapped atoms in free space (*7*, *8*) and in cavities (*9*), and atomic ensembles in the regime of continuous variables (*10*).

An approach of particular importance has been the seminal work of Duan, Lukin, Cirac, and Zoller (DLCZ) for the realization of quantum networks based on entanglement between single photons and collective excitations in atomic ensembles (*11*). Critical experimental capabilities have been achieved, beginning with the generation of nonclassical fields (*12*, *13*) with controlled waveforms (*14*) and extending to the creation and retrieval of single collective excitations (*15*–*17*) with high efficiency (*18*, *19*). Heralded entanglement with quantum memory, which is the cornerstone of networks with efficient scaling, was achieved between two ensembles (*20*). More recently, conditional control of the quantum states of a single ensemble (*21*–*23*) and of two distant ensembles (*24*) has also been implemented; the quantum states are likewise required for the scalability of quantum networks based on probabilistic protocols.

Our goal is to develop the physical resources that enable quantum repeaters (*5*), thereby allowing entanglement-based quantum communication tasks over quantum networks on distance scales much larger than those set by the attenuation length of optical fibers, including quantum cryptography (*25*). For this purpose, heralded number-state entanglement (*20*) between two remote atomic ensembles is not directly applicable. Instead, DLCZ proposed the use of pairs of ensembles (U_i,D_i) at each quantum node i, with the sets of ensembles $\{U_i\},\{D_i\}$ separately linked in parallel chains across the network (*11*). Relative to the state of the art in our previous work (*20*), the DLCZ protocol requires the capability for the independent control of pairs of entangled ensembles between two nodes.

In our experiment, we created, addressed, and controlled pairs of atomic ensembles at each of two quantum nodes, thereby demonstrating entanglement distribution in a form suitable both for quantum network architectures and for entanglement-based quantum communication schemes (*26*). Specifically, two pairs of remote ensembles at two nodes were each prepared in an entangled state (*20*), in a heralded and asynchronous fashion (*24*), thanks to the conditional control of the quantum memories. After a signal indicating that the two chains are prepared in the desired state, the states of the ensembles were coherently transferred to propagating fields locally at the two nodes. The fields were arranged such that they effectively contained two photons, one at each node, whose polarizations were entangled. The entanglement between the two nodes was verified by the violation of a Bell inequality. The effective polarization-entangled state, created with favorable scaling behavior, was thereby compatible with entanglement-based quantum communication protocols (*11*).

The architecture for our experiment is shown in Fig. 1. Each quantum node, L (left) and R (right), consists of two atomic ensembles, U (up) and D (down), or four ensembles altogether, namely (LU, LD) and (RU, RD), respectively. We first prepared each pair in an entangled state, in which one excitation is shared coherently, by using a pair of coherent weak write pulses to induce spontaneous Raman transitions $|g\rangle \rightarrow |e\rangle \rightarrow |s\rangle$ (bottom left, Fig. 1). The Raman fields $(1_{LU},1_{RU})$ from (LU, RU) were

Norman Bridge Laboratory of Physics 12-33, California Institute of Technology, Pasadena, CA 91125, USA.

*Present address: Group of Applied Physics, University of Geneva, Geneva 1211, Switzerland.

†Present address: Departamento de Física, Universidade Federal de Pernambuco, Recife-PE, 50670-901, Brazil.

‡To whom correspondence should be addressed. E-mail: hjkimble@caltech.edu

combined at the 50-50 beamsplitter BS_U, and the resulting fields were directed to single-photon detectors. A photoelectric detection event in either detector indicated that the two ensembles were prepared. The remote pair of D ensembles, (LD, RD), was prepared in an analogous fashion.

Conditioned upon the preparation of both ensemble pairs (LU, LD) and (RU, RD), a set of read pulses was triggered to map the stored atomic excitations into propagating Stokes fields in well-defined spatial modes through $|s\rangle \rightarrow |e\rangle \rightarrow |g\rangle$ with the use of a collective enhancement (*11*) (bottom left, Fig. 1). This generated a set of four fields denoted by (2_{LU},2_{RU}) for ensembles (LU, RU) and by (2_{LD}, 2_{RD}) for ensembles (LD, RD). In the ideal case and neglecting higher-order terms, this mapping results in a quantum state for the Field 2 fields given by

$$|\psi_{2_{LU},2_{RU},2_{LD},2_{RD}}\rangle = \frac{1}{2}(|0\rangle_{2_{LU}}|1\rangle_{2_{RU}} \pm e^{i\eta_U}|1\rangle_{2_{LU}}|0\rangle_{2_{RU}})_U \otimes (|0\rangle_{2_{LD}}|1\rangle_{2_{RD}} \pm e^{i\eta_D}|1\rangle_{2_{LD}}|0\rangle_{2_{RD}})_D \quad (1)$$

Here, $|n\rangle_x$ is the n-photon state for mode x, where $x \in \{2_{LU},2_{RU},2_{LD},2_{RD}\}$, and η_U and η_D are the relative phases resulting from the writing and reading processes for the U and D pair of ensembles, respectively (*20*). The ± signs for the conditional states U,D result from the unitarity of the transformation by the beamsplitters (BS_U, BS_D). The extension of Eq. 1 to incorporate various nonidealities is given in the supporting online material (SOM) text.

Apart from an overall phase, the state $|\psi_{2_{LU},2_{RU},2_{LD},2_{RD}}\rangle$ can be rewritten as follows:

$$|\psi_{2_{LU},2_{RU},2_{LD},2_{RD}}\rangle = \frac{1}{2}[e^{-i\eta_D}|1\rangle_{2_{RU}}|1\rangle_{2_{RD}}|vac\rangle_{2_L} \pm e^{i\eta_U}|1\rangle_{2_{LU}}|1\rangle_{2_{LD}}|vac\rangle_{2_R} \pm (|0\rangle_{2_{LU}}|1\rangle_{2_{LD}}|0\rangle_{2_{RD}}|1\rangle_{2_{RU}} \pm e^{i(\eta_U-\eta_D)}|1\rangle_{2_{LU}}|0\rangle_{2_{LD}}|1\rangle_{2_{RD}}|0\rangle_{2_{RU}})] \quad (2)$$

where $|vac\rangle_{2_i}$ denotes $|0\rangle_{2_{iU}}|0\rangle_{2_{iD}}$. If only coincidences between both nodes L,R are registered, the first two terms (i.e., with $e^{-i\eta_D}$, $e^{i\eta_U}$) do not contribute. Hence, as noted by DLCZ, excluding such cases leads to an effective density matrix equivalent to the one for a maximally entangled state of the form of the last term in Eq. 2. Notably, the absolute phases η_U and η_D do not need to be independently stabilized. Only the relative phase $\eta = \eta_U - \eta_D$ must be kept constant, leading to 1/2 unit of entanglement for two quantum bits (i.e., 1/2 ebit).

The experimental demonstration of this architecture for implementing the DLCZ protocol relies critically on the ability to carry out efficient parallel preparation of the (LU, RU) and (LD, RD) ensemble pairs, as well as the ability to stabilize the relative phase η. The first requirement is achieved by the use of real-time control, as described in Felinto *et al.* (*24*) in a simpler case. As shown in Fig. 1, we implemented control logic that monitors the outputs of Field 1 detectors. A detection event at either pair triggers electro-optic intensity modulators (IM) that gate off all laser pulses traveling toward the corresponding pair of ensembles, thereby storing the associated state. Upon receipt of signals indicating that the two pairs of ensembles, (LU, RU) and (LD, RD), have both been independently prepared, the control logic triggers the retrieval of the stored states by simultaneously sending a strong read pulse into each of the four ensembles. Relative to the case in which no logic is implemented, this process resulted in a 19-fold enhancement in the probability of generating this overall state from the four ensembles (SOM text).

The second requirement—stability of the relative phase η—could be accomplished by active stabilization of each individual phase η_U,η_D, as in (*20*). Instead of implementing this challenging technical task (which ultimately would have to be extended across longer chains of ensembles), our setup exploits the passive stability between two independent polarizations propagating in a single interferometer to prepare the two ensemble pairs (*27*). No active phase stabilization is thus required. In practice, we found that the passive stability of our system was sufficient for operation overnight without adjustment. Additionally, we implemented a procedure that deterministically sets the relative phase η to zero.

We also extended the original DLCZ protocol (Fig. 1) by combining fields (2_{LU}, 2_{LD}) and (2_{RU}, 2_{RD}) with orthogonal polarizations on polarizing beamsplitters PBS_L and PBS_R to yield fields 2_L and 2_R, respectively. The polarization encoding opens the possibility of performing additional entanglement purification and thus superior scalability (*28*, *29*). In the ideal case, the resulting state would now be effectively equivalent to a maximally entangled state for the polarization of two photons

$$|\psi^{\pm}_{2_L,2_R}\rangle_{\text{eff}} \propto |H_{2_L}\rangle|V_{2_R}\rangle \pm e^{i\eta}|V_{2_L}\rangle|H_{2_R}\rangle \quad (3)$$

where $|H\rangle$ and $|V\rangle$ stand for the state of a single photon with horizontal and vertical polarization, respectively. The sign of the superposition in Eq. 3 is inherited from Eq. 1 and is determined by the particular pair of heralding signals recorded by (D_{1a},D_{1b}) and (D_{1c},D_{1d}). The entanglement in the polarization basis is well suited for entanglement-based quantum cryptography (*11*, *25*), including security verifica-

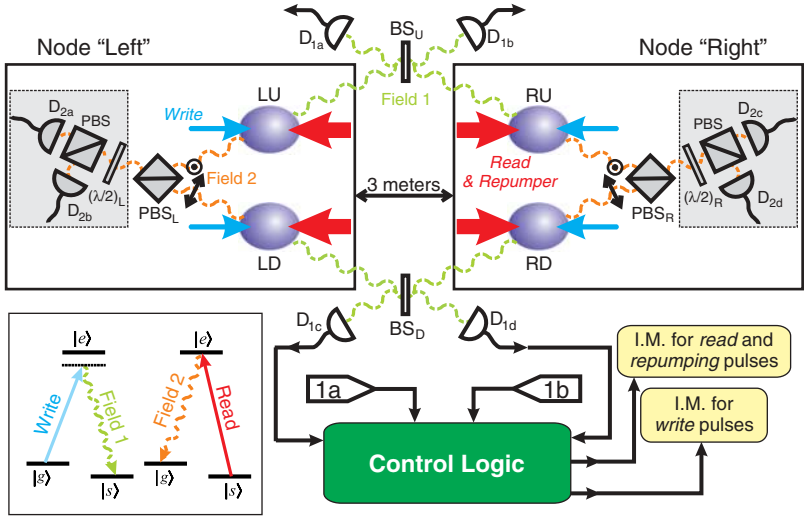

Fig. 1. Setup for distributing entanglement between two quantum nodes (L,R) separated by 3 m. The inset at the bottom left shows the relevant atomic levels for the $6S_{1/2} \rightarrow 6P_{3/2}$ transition in atomic cesium, as well as the associated light fields. The ensembles are initially prepared in $|g\rangle$. Weak write pulses then induce spontaneous Raman transitions $|g\rangle$ ($F = 4$)→$|e\rangle$ ($F' = 4$)→ $|s\rangle$ ($F = 3$), resulting in the emission of anti-Stokes fields (Field 1) near the $|e\rangle \rightarrow |s\rangle$ transition along with the storage of collective excitations in the form of spin-flips shared among the atoms (*11*). With this setup, a photo-detection event at either detector D_{1a} or D_{1b} indicates entanglement between the collective excitation in LU and RU, and a photo-detection event at either detector D_{1c} or D_{1d} indicates entanglement between the collective excitation in LD and RD (*20*). Two orthogonal polarizations in one fiber beamsplitter implement BS_U and BS_D, yielding excellent relative path stability. A heralding detection event triggers the control logic to gate off the light pulses going to the corresponding ensemble pair (U or D) by controlling the intensity modulators (I.M.). The atomic state is thus stored while waiting for the second ensemble pair to be prepared. After both pairs of ensembles U,D are entangled, the control logic releases strong read pulses to map the states of the atoms to Stokes Field 2 fields through $|s\rangle \rightarrow |e\rangle \rightarrow |g\rangle$. Fields 2_{LU} and 2_{LD} are combined with orthogonal polarizations on the polarizing beamsplitter PBS_L to yield field 2_L; fields 2_{RU} and 2_{RD} are combined with orthogonal polarizations on the polarizing beam splitter PBS_R to yield field 2_R. If only coincidences between fields 2_L and 2_R are registered, the state is effectively equivalent to a polarization maximally entangled state.

tion by way of the violation of a Bell inequality, as well as for quantum teleportation (*11*).

As a first step to investigate the joint states of the atomic ensembles, we recorded photoelectric counting events for the ensemble pairs (*LU*,*RU*) and (*LD*,*RD*) by setting the angles for the half-wave plates $(\lambda/2)_{L,R}$ shown in Fig. 1 to 0°, such that photons reaching detectors D_{2b} and D_{2d} come only from the ensemble pair *U*, and photons reaching detectors D_{2a} and D_{2c} come only from the ensemble pair *D*. Conditioned upon detection events at D_{1a} or D_{1b} (or at D_{1c} or D_{1d}), we estimated the probability that each ensemble pair *U*,*D* contains only a single, shared excitation as compared with the probability for two excitations by way of the associated photoelectric statistics. In quantitative terms, we determined the ratio (*20*)

$$h_X^{(2)} \equiv \frac{p_{X,11}}{p_{X,10}p_{X,01}} \quad (4)$$

where $p_{X,mn}$ is the probability to register *m* photodetection events in mode 2_{LX} and *n* events in mode 2_{RX} ($X = \{U,D\}$), conditioned on a detection event at D_1. A necessary condition for the two ensembles (*LX*, *RX*) to be entangled is that $h_X^{(2)} < 1$, where $h_X^{(2)} = 1$ corresponds to the case of independent (unentangled) coherent states for the two fields (*20*). Figure 2 shows the measured $h_X^{(2)}$ versus the duration τ_M (where M stands for memory) that the state is stored before retrieval. For both *U* and *D* pairs, $h^{(2)}$ remains well below unity for storage times $\tau_M < \sim 10$ μs. For the *U* pair, the solid line in Fig. 2 provides a fit by the simple expression $h^{(2)} = 1 - A\exp[-(\tau_M/\tau)^2]$. The fit gives $A = 0.94 \pm 0.01$, where the error is SD, and $\tau = 22 \pm 2$ μs, providing an estimate of a coherence time for our system. A principal cause for decoherence is an inhomogeneous broadening of the ground state levels by residual magnetic fields (*30*). The characterization of the time dependence of $h^{(2)}$ constitutes an important benchmark of our system (SOM text).

We next measured the correlation function $E(\theta_L,\theta_R)$, defined by

$$E(\theta_L,\theta_R) = \frac{C_{ac} + C_{bd} - C_{ad} - C_{bc}}{C_{ac} + C_{bd} + C_{ad} + C_{bc}} \quad (5)$$

Here, C_{jk} gives the rates of coincidences between detectors D_{2j} and D_{2k} for Field 2 fields, where $j,k \in \{a,b,c,d\}$, conditioned upon heralding events at detectors D_{1a},D_{1b} and D_{1c},D_{1d} from Field 1 fields. The angles of the two half-wave plates $(\lambda/2)_L$ and $(\lambda/2)_R$ are set at $\theta_L/2$ and $\theta_R/2$, respectively. As stated above, the capability to store the state heralded in one pair of ensembles and then to wait for the other pair to be prepared markedly improves the various coincidence rates C_{jk} by a factor that increases with the duration τ_M that a state can be preserved (*24*) (SOM text).

Figure 3 displays the correlation function *E* as a function of θ_R, for $\theta_L = 0°$ (Fig. 3A) and $\theta_L = 45°$ (Fig. 3B). Relative to Fig. 2, these data are taken with increased excitation probability (higher write power) to validate the phase stability of the system, which is evidently good. Moreover, these four-fold coincidence fringes in Fig. 3A provide further verification that predominantly one excitation is shared between a pair of ensembles. The analysis provided in the SOM text with the measured cumulative $h^{(2)}$ parameter for this set of data, $h^{(2)} = 0.12 \pm 0.02$, predicts a visibility of $V = 78 \pm 3\%$ in good agreement with the experimentally determined $V \cong 75\%$. Finally, one of the fringes is inverted with respect to the other in Fig. 3B, which corresponds with the two possible signs in Eq. 3.

As for $\theta_L = 45°$, the measurement is sensitive to the square of the overlap ξ of photon wavepackets for fields $2_{U,D}$; we may infer $\xi_{U,D} \cong 0.85$ from the reduced fringe visibility ($V \cong 55\%$) in Fig. 3B relative to Fig. 3A, if all the reduction is attributed to a nonideal overlap. An independent experiment for two-photon interference in this setup has shown an overlap $\xi \cong 0.90$, which confirms that the reduction can be principally attributed to the nonideal overlap. Other possible causes include imperfect phase alignment $\eta \neq 0$ and imbalance of the effective-state coefficients (SOM text).

With the measurements from Figs. 2 and 3 in hand, we verified entanglement unambiguously

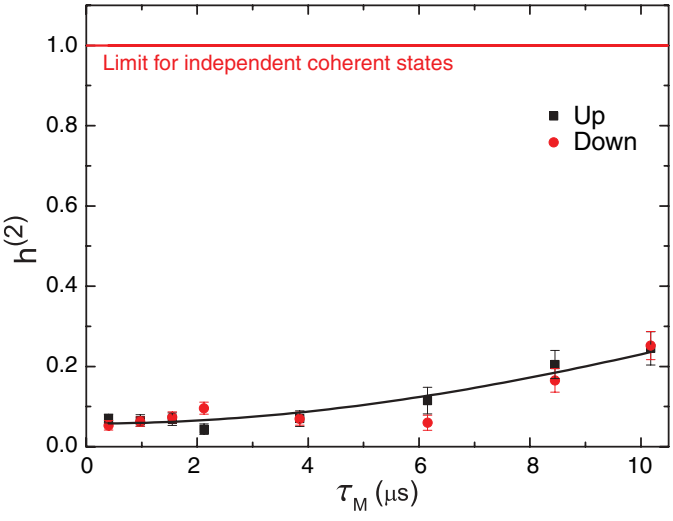

Fig. 2. Suppression $h^{(2)}$ of the probabilities for each ensemble to emit two photons compared with the product of the probabilities that only one photon is emitted, as a function of the duration τ_M that the state is stored before retrieval. The solid line gives a fit for the *U* pair. Error bars indicate SD.

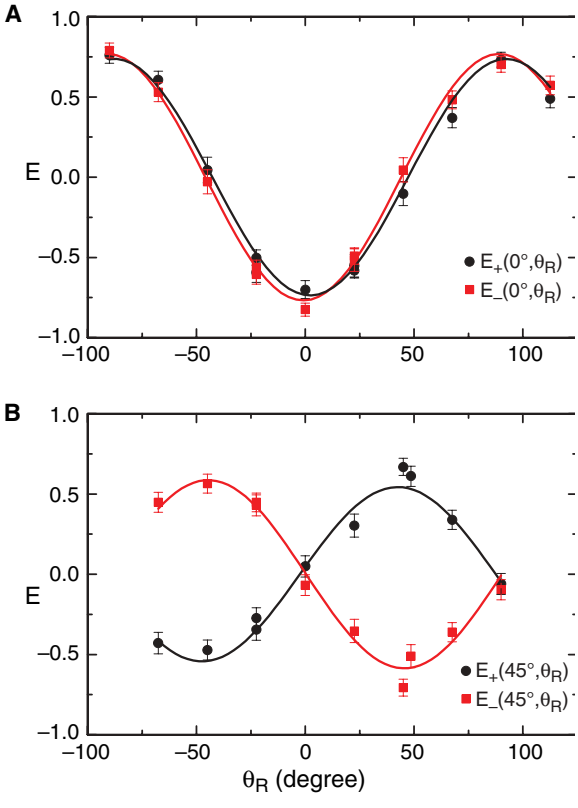

Fig. 3. Measured correlation function $E(\theta_L, \theta_R)$ as a function of θ_R with θ_L fixed at (**A**) 0° and (**B**) 45°. The excitation probabilities for the ensembles are increased by ~1.5 times relative to Fig. 2, with each point taken for 30 min at a typical coincidence rate of 400 per hour for each fringe. Error bars indicate SD.

by way of the violation of a Bell inequality (*31*). For this purpose, we chose the canonical values, $\theta_L = \{0°,45°\}$ and $\theta_R = \{22.5°,-22.5°\}$, and constructed the Clauser-Horne-Shimony-Holt (CHSH) parameters

$$S_+ \equiv |E(0^\circ, 22.5^\circ) + E(0^\circ, -22.5^\circ) + E(45^\circ, -22.5^\circ) - E(45^\circ, 22.5^\circ)| \quad (6)$$

$$S_- \equiv |E(0^\circ, 22.5^\circ) + E(0^\circ, -22.5^\circ) + E(45^\circ, 22.5^\circ) - E(45^\circ, -22.5^\circ)| \quad (7)$$

for the two effective states $|\psi_{2_L,2_R^\pm}\rangle_{\text{eff}}$ in Eq. 3. For local, realistic hidden-variable theories, $S_\pm \leq 2$ (*31*). Figure 4 shows the CHSH parameters $S_\pm$ as functions of the duration τ_M up to which one pair of ensembles holds the prepared state, in the excitation regime of Fig. 2. As shown in the SOM text, the requirements for minimization of higher-order terms are much more stringent in this experiment with four ensembles than with simpler configurations (*21*).

Figure 4, A and B, gives the results for our measurements of $S_\pm$ with binned data. Each point corresponds to the violation obtained for states generated at $\tau_M \pm \Delta\tau_M/2$ ($\Delta\tau_M$ is marked by the thick horizontal lines in Fig. 4). Strong violations are obtained for short memory times—for instance, $S_+ = 2.55 \pm 0.14 > 2$ and $S_- = 2.61 \pm 0.13 > 2$ for the second bin—demonstrating the presence of entanglement between fields 2_L and 2_R. Therefore, these fields can be exploited to perform entanglement-based quantum communication protocols, such as quantum key distribution with, at minimum, security against individual attacks (*11*, *32*).

As can be seen in Fig. 4, the violation decreases with increasing τ_M. The decay is largely due to the time-varying behavior of $h^{(2)}$ (Fig. 2 and SOM text). In addition to this decay, the S_+ parameter exhibits modulation with τ_M. We explored different models for the time dependence of the CHSH parameters, but thus far have found no satisfactory agreement between model calculations and measurements. Nevertheless, the density matrix for the ensemble over the full memory time is potentially useful for tasks such as entanglement connection, as shown by Fig. 4, C and D, in which cumulative data are given. Each point at memory time τ_M gives the violation obtained by taking into account all the states generated from 0 to τ_M. Overall significant violations are obtained, namely $S_+ = 2.21 \pm 0.04 > 2$ and $S_- = 2.24 \pm 0.04 > 2$ at $\tau_M \sim 10\ \mu s$.

In our experiment, we were able to generate excitation-number entangled states between remote locations, which are well suited for scaling purposes, and, with real-time control, we were able to operate them as if they were effectively polarization-entangled states, which can be applied to quantum communications such as quantum cryptography. Measurements of the suppression $h^{(2)}$ of two-excitation components versus storage time explicitly demonstrates the major source that causes the extracted polarization entanglement to decay, emphasizing the critical role of multi-excitation events in the experiments aiming for a scalable quantum network. The present scheme, which constitutes a functional segment of a quantum repeater in terms of quantum state encoding and channel control, allows the distribution of entanglement between two quantum nodes. The extension of our work to longer chains involving many segments becomes more complicated and is out of reach for any current system. For long-distance communication, the first quantity to improve is the coherence time of the memory. Better cancellation of the residual magnetic fields and switching to new trap schemes should improve this parameter to ~0.1 s by using an optical trap (*30*), thereby increasing the rate of preparing the ensembles in the state of Eq. 1 to ~100 Hz. The second challenge that would immediately appear in an extended chain would be the increase of the multi-excitation probability with the connection stages. Recently, Jiang *et al.* (*28*) have theoretically demonstrated the prevention of such growth in a similar setup, but its full scalability still requires very high retrieval and detection efficiency, and photon-number resolving detectors. These two points clearly show that the quest of scalable quantum networks is still a theoretical and experimental challenge. The availability of our first functional segment opens the way for fruitful investigations.

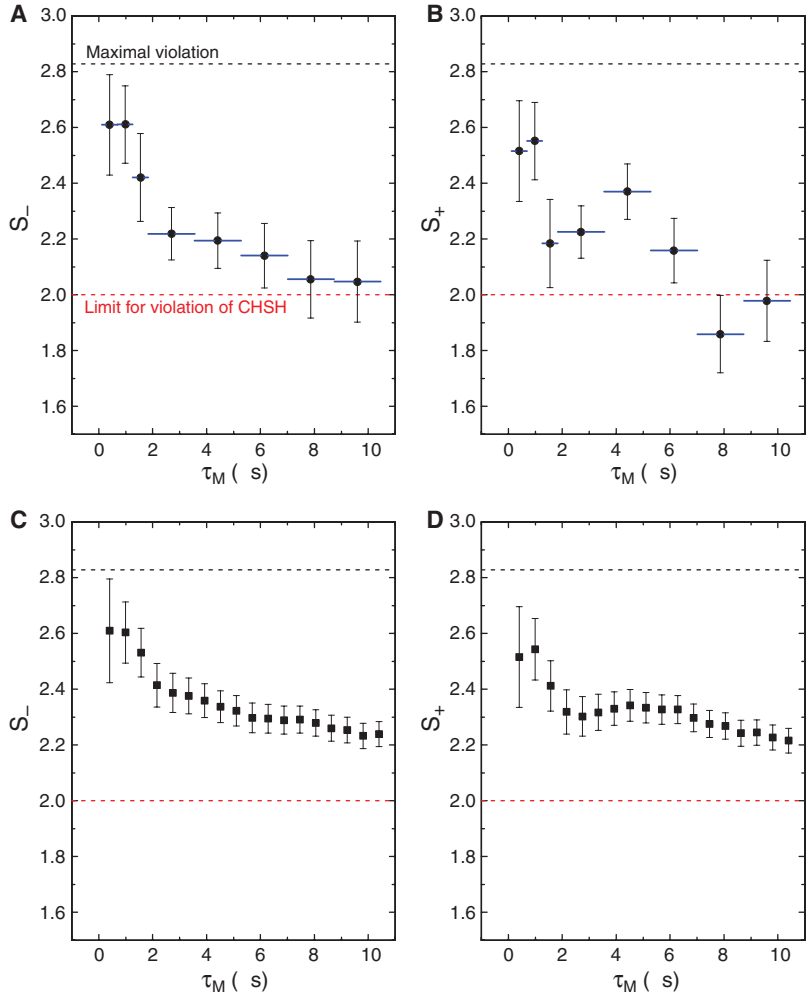

Fig. 4. Measured CHSH parameters $S_\pm$, for the two possible effective states in Eq. 3, as functions of duration τ_M for which the first ensemble pair holds the prepared state. The excitation probabilities are kept low for high correlation (as in Fig. 2). (**A** and **B**) Binned data. The horizontal solid lines indicate the size of the bins used. (**C** and **D**) Cumulative data. The coincidence rate for these measurements is about 150 per hour for each effective state. Error bars indicate SD.

References and Notes

1. P. Zoller *et al.*, *Eur. Phys. J. D* **36**, 203 (2005).
2. V. Giovannetti, S. Lloyd, L. Maccone, *Science* **306**, 1330 (2004).
3. J. I. Cirac, P. Zoller, H. J. Kimble, H. Mabuchi, *Phys. Rev. Lett.* **78**, 3221 (1997).
4. L.-M. Duan, H. J. Kimble, *Phys. Rev. Lett.* **92**, 127902 (2004).
5. H.-J. Briegel, W. Dür, J. I. Cirac, P. Zoller, *Phys. Rev. Lett.* **81**, 5932 (1998).
6. B. B. Blinov, D. L. Moehring, L.-M. Duan, C. Monroe, *Nature* **428**, 153 (2004).
7. J. Volz *et al.*, *Phys. Rev. Lett.* **96**, 030404 (2006).
8. J. Beugnon *et al.*, *Nature* **440**, 779 (2006).

9. A. D. Boozer, A. Boca, R. Miller, T. T. Northup, H. J. Kimble, *Phys. Rev. Lett.*, in press; preprint available at http://xxx.lanl.gov/abs/quant-ph/0702248.
10. J. F. Sherson *et al.*, *Nature* **443**, 557 (2006).
11. L.-M. Duan, M. Lukin, J. I. Cirac, P. Zoller, *Nature* **414**, 413 (2001).
12. A. Kuzmich *et al.*, *Nature* **423**, 731 (2003).
13. C. H. van der Wal *et al.*, *Science* **301**, 196 (2003).
14. V. Balić, D. A. Braje, P. Kolchin, G. Y. Yin, S. E. Harris, *Phys. Rev. Lett.* **94**, 183601 (2005).
15. C.-W. Chou, S. V. Polyakov, A. Kuzmich, H. J. Kimble, *Phys. Rev. Lett.* **92**, 213601 (2004).
16. M. D. Eisaman *et al.*, *Nature* **438**, 837 (2005).
17. T. Chanelière *et al.*, *Nature* **438**, 833 (2005).
18. J. Laurat *et al.*, *Opt. Express* **14**, 6912 (2006).
19. J. K. Thompson, J. Simon, H. Loh, V. Vuletić, *Science* **313**, 74 (2006).
20. C.-W. Chou *et al.*, *Nature* **438**, 828 (2005).
21. H. de Riedmatten *et al.*, *Phys. Rev. Lett.* **97**, 113603 (2006).
22. D. N. Matsukevich *et al.*, *Phys. Rev. Lett.* **97**, 013601 (2006).
23. S. Chen *et al.*, *Phys. Rev. Lett.* **97**, 173004 (2006).
24. D. Felinto *et al.*, *Nat. Phys.* **2**, 844 (2006).
25. A. K. Ekert, *Phys. Rev. Lett.* **67**, 661 (1991).
26. Materials and methods are available as supporting material on *Science* Online.
27. C.-W. Chou, thesis, California Institute of Technology, Pasadena, CA (2006); (http://etd.caltech.edu/etd/available/etd-05252006-185918/unrestricted/thesis.pdf).
28. L. Jiang, J. M. Taylor, M. D. Lukin, *Quant. Phys.*, in press; preprint available at http://xxx.lanl.gov/abs/quant-ph/0609236.
29. Z. B. Chen, B. Zhao, J. Schmiedmayer, J.-W. Pan, *Quant. Phys.*, in press; preprint available at http://xxx.lanl.gov/abs/quant-ph/0609151.
30. D. Felinto, C.-W. Chou, H. de Riedmatten, S. V. Polyakov, H. J. Kimble, *Phys. Rev. A.* **72**, 053809 (2005).
31. J. F. Clauser, A. Shimony, *Rep. Prog. Phys.* **41**, 1881 (1978).
32. C. A. Fuchs, N. Gisin, R. B. Griffiths, C. S. Niu, A. Peres, *Phys. Rev. A.* **56**, 1163 (1997).

33. We gratefully acknowledge critical discussions with S. J. van Enk. This research is supported by the Disruptive Technologies Office and by the NSF. J.L. acknowledges financial support from the European Union (Marie Curie fellowship). H.D. acknowledges support as Fellow of the Center for the Physics of Information at the California Institute of Technology.

Supporting Online Material

www.sciencemag.org/cgi/content/full/1140300/DC1
Materials and Methods
SOM Text
Figs. S1 to S3
Table S1
References

23 January 2007; accepted 27 March 2007
Published online 5 April 2007;
10.1126/science.1140300
Include this information when citing this paper.

Anisotropic Violation of the Wiedemann-Franz Law at a Quantum Critical Point

Makariy A. Tanatar,[1,2]*† Johnpierre Paglione,[2,3]* Cedomir Petrovic,[4] Louis Taillefer[1,5]‡

A quantum critical point transforms the behavior of electrons so strongly that new phases of matter can emerge. The interactions at play are known to fall outside the scope of the standard model of metals, but a fundamental question remains: Is the basic concept of a quasiparticle—a fermion with renormalized mass—still valid in such systems? The Wiedemann-Franz law, which states that the ratio of heat and charge conductivities in a metal is a universal constant in the limit of zero temperature, is a robust consequence of Fermi-Dirac statistics. We report a violation of this law in the heavy-fermion metal $CeCoIn_5$ when tuned to its quantum critical point, depending on the direction of electron motion relative to the crystal lattice, which points to an anisotropic destruction of the Fermi surface.

Discovered in 1853, the Wiedemann-Franz (WF) law (*1*) has stood as a robust empirical property of metals, whereby the thermal conductivity κ of a sample is related to its electrical conductivity σ through a universal ratio. In 1927, Sommerfeld (*2*) used quantum mechanics, applying to electrons the new Fermi-Dirac statistics, to derive the following theoretical relation

$$\frac{\kappa}{\sigma T} = \frac{\pi^2}{3}\left(\frac{k_B}{e}\right)^2 \qquad (1)$$

where T is the absolute temperature, k_B is Boltzmann's constant and e is the charge of the electron. The extremely good agreement between the theoretical constant $L_0 \equiv \frac{\pi^2}{3}\left(\frac{k_B}{e}\right)^2$ and the empirical value played a pivotal role in establishing the quantum theory of solids. In 1957, Landau went on to show that, even in the presence of strong interactions, electrons in a metal can still be described as weakly interacting fermions ("quasiparticles") with renormalized mass (*3*). This is the essence of what became known as Fermi-liquid (FL) theory, the "standard model" of metals. In the limit of zero temperature, the WF law survived unchanged because it does not depend on mass. (Eq. 1 is only a law at $T \to 0$, as only in that limit is energy conserved in collisions.) It has since been shown that the WF law remains valid as $T \to 0$ for arbitrary strong scattering, disorder, and interactions (*4*). It is built into the fabric of matter, valid down to the quanta of conductance, respectively equal to $\frac{\pi^2}{3}\frac{k_B{}^2 T}{h}$ for heat and $\frac{e^2}{h}$ for charge (*5*).

In the past decade, however, departures from FL theory have been observed in *d*- and *f*-electron metals when tuned to a quantum critical point (QCP), a zero-temperature phase transition between distinct electronic ground states (*6*). These typically show up as an anomalous temperature dependence of properties at the QCP, for example, a specific heat coefficient that never saturates, growing as $C/T \sim \log(1/T)$ (*7*), and an electrical resistivity that grows linearly with T (*8*). Quantum criticality also appears to be linked to the emergence of exotic forms of superconductivity (*9*–*11*) and nematic (*12*) electronic states of matter.

To determine whether Landau quasiparticles survive at a QCP, we have measured the transport of heat and charge in $CeCoIn_5$, a heavy-fermion metal with a QCP tuned by magnetic field H. In its phase diagram (Fig. 1), the QCP is located on the border of superconductivity and marks the end of a FL regime at $H = H_c = 5.0$ T, where the electrical resistivity obeys the FL form $\rho = \rho_0 + AT^2$ (*13*). A power-law fit to the A coefficient yields $A \sim (H - H_c)^{-\alpha}$, with $\alpha \cong 4/3$ and $H_c = 5.0 \pm 0.1$ T (*13*). At H_c, C/T never saturates (*14*). The same phenomenology is found at the field-tuned QCP of $YbRh_2Si_2$ (with $\alpha \cong 1$) (*15*).

In Fig. 2, we show how the thermal and electrical resistivities in the $T = 0$ limit behave in $CeCoIn_5$ as the field is tuned toward H_c. These are extrapolations to $T = 0$ of the low-temperature thermal resistivity, defined as $w \equiv L_0 T/\kappa$, and electrical resistivity ρ, for current directions parallel ($J \parallel c$) and perpendicular ($J \perp c$) to the tetragonal axis of the crystal lattice. The raw data and their extrapolation are shown in detail in (*4*). For $H = 10$ T, far away from H_c, $w(T)$ and $\rho(T)$ converge as $T \to 0$ for both current directions. However, very close to the QCP, for $H = 5.3$ T, they only converge for in-plane transport. In other words, transport along the c axis violates the WF law, with w_c extrapolating to a distinctly larger value than ρ_c as $T \to 0$. In the supporting material (*4*), we show that extrapolations are not needed to conclude in a violation of the WF law, as the difference data, $w_c(T) - \rho_c(T)$ versus T, shows a rigid T-independent shift from field to field. The normalized Lorenz ratio, $\frac{L}{L_0} \equiv \frac{\kappa}{L_0 \sigma} \equiv \frac{\rho}{w}$, is also seen to approach unity at 10 T but not at 5.3 T.

Our observation of a violation of the WF law at a QCP is characterized by three distinctive

[1]Département de Physique et RQMP, Université de Sherbrooke, Sherbrooke, Canada. [2]Department of Physics, University of Toronto, Toronto, Canada. [3]Department of Physics, University of California, San Diego, CA 92093, USA. [4]Condensed Matter Physics and Materials Science Department, Brookhaven National Laboratory, Upton, NY 11973, USA. [5]Canadian Institute for Advanced Research, Toronto, Canada.

*These authors contributed equally to this work.
†Present address: Institute of Surface Chemistry, National Academy of Sciences of Ukraine, Kyiv, Ukraine.
‡To whom correspondence should be addressed. E-mail: louis.taillefer@physique.usherbrooke.ca